

# Efficient Masked Autoencoders with Self-Consistency

Zhaowen Li<sup>1,2</sup> Yousong Zhu<sup>1</sup> Zhiyang Chen<sup>1,2</sup> Wei Li<sup>3</sup> Chaoyang Zhao<sup>1</sup> Liwei Wu<sup>3</sup>  
Rui Zhao<sup>3</sup> Ming Tang<sup>1</sup> Jinqiao Wang<sup>1,2,4</sup>

National Laboratory of Pattern Recognition, Institute of Automation, CAS, Beijing, China<sup>1</sup>  
School of Artificial Intelligence, University of Chinese Academy of Sciences, Beijing, China<sup>2</sup>  
SenseTime Research<sup>3</sup> Peng Cheng Laboratory, Shenzhen, China<sup>4</sup>

{zhaowen.li, yousong.zhu, zhiyang.chen, chaoyang.zhao, tangm, jqwang}@nlpr.ia.ac.cn  
{liweil, wuliwei, zhaorui}@sensetime.com

## Abstract

Inspired by masked language modeling (MLM) in natural language processing, masked image modeling (MIM) has been recognized as a strong and popular self-supervised pre-training method in computer vision. However, its high random mask ratio would result in two serious problems: 1) the data are not efficiently exploited, which brings inefficient pre-training (e.g., 1600 epochs for MAE vs. 300 epochs for the supervised), and 2) the high uncertainty and inconsistency of the pre-trained model, i.e., the prediction of the same patch may be inconsistent under different mask rounds. To tackle these problems, we propose efficient masked autoencoders with self-consistency (EMAE), to improve the pre-training efficiency and increase the consistency of MIM. In particular, we progressively divide the image into  $K$  non-overlapping parts, each of which is generated by a random mask and has the same mask ratio. Then the MIM task is conducted parallelly on all parts in an iteration and generates predictions. Besides, we design a self-consistency module to further maintain the consistency of predictions of overlapping masked patches among parts. Overall, the proposed method is able to exploit the data more efficiently and obtains reliable representations. The experiments on ImageNet show that EMAE achieves even higher results with only 300 pre-training epochs under ViT-Base than MAE (1600 epochs). EMAE also consistently obtains state-of-the-art transfer performance on various downstream tasks, like object detection, and semantic segmentation.

## 1. Introduction

Self-supervised learning in computer vision (CV) [1, 2, 4–6, 8, 18–20, 30, 46] is widely used to learn general repre-

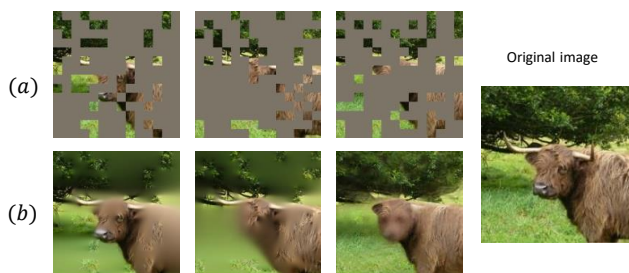


Figure 1. **Different reconstruction results of MAE [19] correspond to different mask seeds.** (a) Different combinations sampled by different mask seeds. (b) Reconstruction results of MAE. For the three reconstructions of (b), only the first represents a normal cattle, and the third even reconstructs a dog. The semantics of these reconstructions by MAE are inconsistent.

sentations from large-scale unlabeled images without relying on human annotations. Generally, massive pretext tasks [1, 2, 4–6, 8, 14, 18–20, 23, 30, 40, 48, 53] are defined for learning unsupervised visual features. Among them, inspired by the success of masked language modeling (MLM) [12], MIM is proposed for pre-training in CV and has shown a preponderant advantage in performance. Commonly, the random mask ratio of MIM is much higher than that of MLM due to the difference in the information density of image and language data [19] (e.g. MAE [19] adopts 75% mask ratio while BERT [12] uses 15% mask ratio). However, we observe that the high random mask ratio will bring two serious problems: 1) images are not exploited efficiently resulting in inefficient pre-training, and 2) the high uncertainty and inconsistency of the pre-trained model.

Here we take MAE and BERT as examples of MIM and MLM, respectively. First, MAE only exploits 25% of the whole image to train the model in a single epoch. Contrastively, BERT uses 85% of the text corpus. Due to in-

sufficient data utilization of MIM, the pre-training epochs commonly are higher than MLM. (*e.g.*, 1600 epochs for MAE *vs.* 40 epochs for MLM in NLP), and the number of pre-training epochs is too large. The reason for this phenomenon is not only the difference in image and language data, but also the difference in the utilization of data between the MLM and MIM methods. Besides, the pre-training efficiency of MIM is still not comparable to that of the supervised (300 epochs for the supervised). Second, the high mask ratio will introduce less reliable features. Hence, different combinations of random visible patches sampled from the original images may generate inconsistent predictions for the same masked patch. As shown in Figure 1, MAE generates different reconstruction results corresponding to different mask seeds, and the semantics of different results are inconsistent.

Is it possible to reduce the random mask ratio to increase pre-training efficiency and improve consistency? In fact, the prior work [19] already shows that reducing the mask ratio brings lower transfer ability for downstream tasks. Therefore, it is essential to design an efficient learning paradigm and reduce the uncertainty of MIM. In this work, we propose efficient masked autoencoders with self-consistency (EMAE), which aims to enhance the pre-training efficiency and increase the certainty and consistency of MIM. Concretely, we first progressively divide the image into  $K$  random non-overlapping parts with the same number of image patches by random mask, and each part performs the MIM task parallelly. The design can effectively improve the pre-training efficiency. Furthermore, a self-consistency module is introduced to encourage the model to output reliable representations under different input visible patches.

We validate our method on multiple visual downstream tasks. With only 300 pre-training epochs, our method outperforms MAE with 1600 pre-training epochs by 0.4% on the ImageNet linear evaluation protocol under ViT-base [14]. Our 800-epoch classification results using ViT-large are comparable with that of 1600-epoch MAE using ViT-huge, it achieves state-of-the-art (SOTA) performance. Moreover, under the architecture of ViT-base, EMAE achieves 54.8% bbox mAP and 47.6% mask mAP using ViTDet [28] on COCO [34] object detection and instance segmentation. Also, EMAE obtains 49.3% mIoU using UperNet [47] on ADE20K [52] semantic segmentation. Overall, we make the following contributions:

- We theoretically prove the high random mask ratio of MIM leads to two serious problems: inefficient pre-training and high inconsistency.
- We propose efficient masked autoencoders with self-consistency to effectively improve pre-training efficiency and obtain reliable representations in MIM.
- Massive experiments demonstrate the effectiveness and

stronger generalization ability of our method. In particular, EMAE outperforms previous SOTA methods in various downstream tasks.

## 2. Related Work

Self-supervised learning builds general representations by exploiting the internal priors or structures of data. These representations can be transferred to various downstream tasks and improve the performance of these tasks. Self-supervised methods in computer vision were based on pre-text tasks [1, 2, 4–6, 8, 14, 18–20, 23, 26, 30, 39–41, 46, 48, 50, 53]. A milestone in self-supervised learning was the contrastive learning/instance discrimination [2, 5, 6, 8, 18, 20, 46]. Besides, mask image modeling [1, 4, 14, 19, 30, 48, 53] is currently the focus of the research community.

### 2.1. Contrastive learning

The learning objective of contrastive learning/instance discrimination is simply to learn representations by distinguishing each image from others, and this approach has proved the excellent performance on extensive downstream tasks, such as image classification [11, 22], object detection [33, 42] and segmentation [21]. The pioneering work [46] proposes to use a memory bank to store the instance class representation vector. MoCo [20] improves the training of instance discrimination methods by storing representations from a momentum encoder instead of the trained network. SimCLR [5] shows that the memory bank can be entirely replaced with the elements from the same batch if the batch is large enough. Meanwhile, BYOL [18] proposes an asymmetric structure and directly bootstraps the representations by attracting the different features from the same instance. Moreover, MoCo v3 [9] applies the practice of contrastive learning in convolutional neural networks to ViT [14] architecture. DINO [3] utilizes knowledge distillation together with ViT in the contrastive learning framework. Nevertheless, much of their progress has far been limited to single-centric-object pre-training data such as ImageNet [11] due to the prior of image semantic consistency [31, 35].

### 2.2. Masked image modeling

With the development of vision Transformer [10, 14] and the success of MLM paradigm in NLP [12], MIM becomes the focus of the research community. MST [30] is the first to introduce MIM into the siamese structure and propose an attention-guided mask strategy. iBOT [53] also adopts the siamese structure and acquires impressive performance. However, these work are built on contrastive learning. The prior work [4] operates on sequences of pixels and predicts unknown pixels. ViT [14] also attempts to study masked patch prediction for self-supervised learning. Following ViT, SimMIM [48] proposes to predict pixels. Moreover,

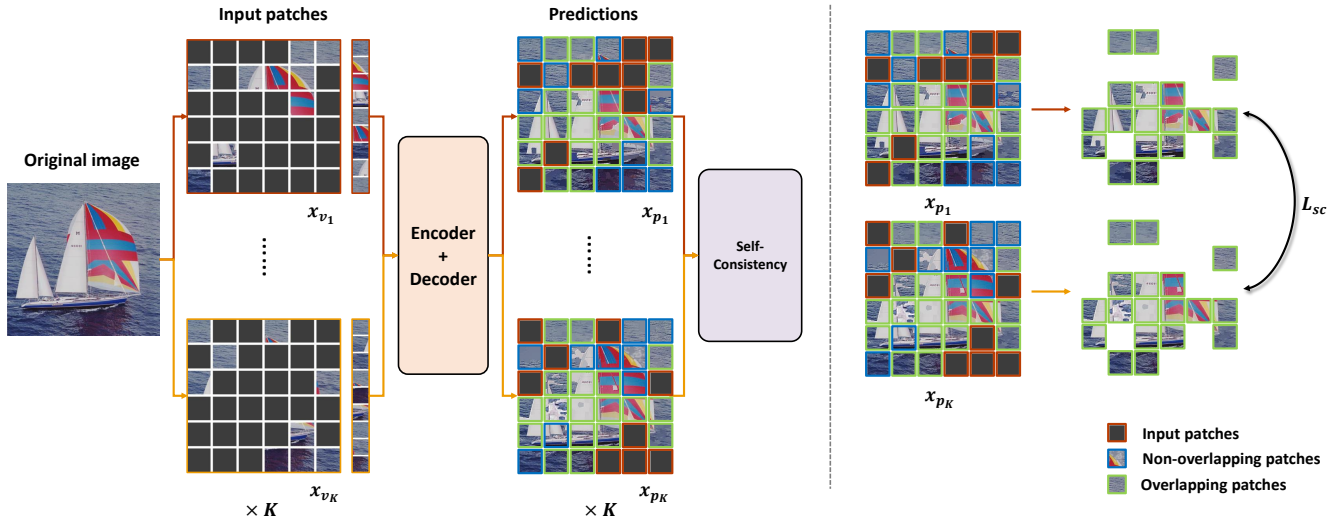


Figure 2. **Illustration of our EMAE.** The whole image is first progressively divided into  $K$  non-overlapping parts  $\mathbf{x}_{v_1}, \dots, \mathbf{x}_{v_K}$  by random mask, and each part has the same number of visible patches. Then, each part is fed into the encoder-decoder architecture and performs the MIM task to generate  $\mathbf{x}_{m_1}, \dots, \mathbf{x}_{m_K}$ . Furthermore, the self-consistency module guides the overlapping patches of predictions among parts to be pulled together. Here, we take  $\mathbf{x}_{p_1}$  and  $\mathbf{x}_{p_K}$  as examples.

BEiT [1] proposes to predict discrete tokens, and its performance depends on the performance of the pre-trained model VQVAE [45]. It is noted that MAE [19] proposes an asymmetric encoder-decoder architecture for the MIM task and shows excellent performance in a variety of visual downstream tasks. However, the mask ratio of MIM is commonly high and this results in two serious problems, namely insufficient pre-training and inconsistency of the pre-trained model. To overcome these problems, we propose efficient masked autoencoders with self-consistency to improve pre-training efficiency and consistency of MIM.

### 2.3. Autoregressive image encoding

Compared with MIM pre-training for ViT, GPT-like autoregressive models [4, 24] in CV can utilize the whole image to perform the self-supervised task. However, the kind of method does not show superior performance and has quadratic time/space complexity of self-attention.

## 3. Method

In this section, we propose an efficient masked autoencoder with self-consistency (EMAE) to learn visual representations, and the pipeline of our proposed method is shown in Figure 2. According to our EMAE, the design of whole data utilization can improve pre-training efficiency in MIM. Besides, the self-consistency module is proposed to reduce the uncertainty and inconsistency of MIM. Therefore, we first give preliminaries about MAE in 3.1, which is adopted as our baseline of MIM. Then, we introduce the design of our proposed EMAE, which boosts both the learn-

ing efficiency and performance in 3.2. Finally, we discuss how the proposed approach will affect the efficiency and performance in 3.3.

### 3.1. Preliminaries about MAE

MAE is a highly recognized MIM framework for self-supervised learning, which gradually incorporates some of the impressive practice in the area. Specifically, according to the pioneering work [19], given a natural image from an unlabeled dataset  $\mathbf{X}$ , we divide it into  $N$  regular image patches, denoted as  $\mathbf{x} \in \mathbf{R}^{N \times S}$  where  $S$  denotes the patch size (e.g.  $16 \times 16$  in ViT [14]). Then, we let  $\mathbf{m} = (m_1, \dots, m_N)$  denote a binary vector of length  $N$ , where  $m_a \in \{0, 1\}$  and  $a \in \{1, 2, \dots, N\}$ , representing the mask over the image, and generating two complementary combinations of  $\mathbf{x}$ : masked patches  $\mathbf{x}_m$  and the visible patches  $\mathbf{x}_v$  are given with Eq(1), where  $\eta = N \times p$  and  $\kappa = N \times (1 - p)$ .

$$\mathbf{x}_m = \mathbf{x} \odot \mathbf{m} \in \mathbf{R}^{\eta \times S}, \mathbf{x}_v = \mathbf{x} \odot (1 - \mathbf{m}) \in \mathbf{R}^{\kappa \times S}, \quad (1)$$

The MAE model  $h = g \circ f$  is an encoder-decoder architecture, we fed these visible patches into encoder  $f(\cdot)$  (e.g., ViT-base), and obtain the latent features. Then, a decoder  $g(\cdot)$  maps the latent feature back to the pixel space to reconstruct the complementary combination and obtain the prediction  $\mathbf{x}_p$ . In particular, MAE minimizes the mean squared error (MSE) between the reconstructed and masked image patches  $\mathbf{x}_m$ , and the loss function is shown as Eq(2).

$$\mathcal{L}_{\text{MAE}}(\mathbf{x}) = \mathcal{L}(\mathbf{x}_v, \mathbf{x}_m) = \mathbb{E} \|g(f(\mathbf{x}_v)) - \mathbf{x}_m\|^2, \quad (2)$$

### 3.2. Efficient MAE with self-consistency

In this section, with MAE as the baseline, we introduce EMAE, a simple method that can greatly improve the pre-training efficiency and obtain reliable representations. An overview of EMAE is shown in Figure 2. EMAE makes two modifications: 1) exploits the whole data, and 2) designs the self-consistency module. In the following, we illustrate the method we proposed in detail.

#### 3.2.1 The utilization of whole data

As described in Eq(1), the random mask ratio is  $p$ , thus the data utilization is  $1 - p$ . That is, the higher the random mask ratio, the lower the data utilization. The low data utilization leads to insufficient data training and decreases the pre-training efficiency. Here we take MAE and BERT as MIM and MLM examples, the ratio of data utilization of MLM to MIM is  $(\frac{17}{5})^M$  if MLM and MIM are pre-trained with the same  $M$  epochs. The high mask ratio makes MAE unable to fully exploit the whole data, thus reducing the pre-training efficiency. Besides, training a model with 1600 epochs consumes a lot of resources and time for the general academic community. For reducing the training epochs and increasing the pre-training efficiency, it is crucial to sufficiently utilize the data. Therefore, we exploit the whole data to train the model, thereby increasing the data utilization.

Concretely, the whole image is first divided into  $N$  image patches. Then, the tensor  $\mathbf{t}$  with random values of length  $N$  is generated, and each value of the tensor fits the uniform distribution on the interval  $[0, 1]$ . The tensor is sorted in ascending order by value and the sorted indices  $\mathbf{ids}$  are obtained as Eq(3), where  $s(\cdot)$  returns the indices that sort a tensor in ascending order by value.

$$\mathbf{ids} = s(\mathbf{t}), \quad (3)$$

Here, we divide the sorted indices of length  $N$  equally into  $K$  non-overlapping parts  $\mathbf{ids}_1, \mathbf{ids}_2, \dots$ , and  $\mathbf{ids}_K$  as shown in Eq(4), where  $i \in \{1, 2, \dots, K\}$ .

$$\mathbf{ids}_i = \mathbf{ids}[(i - 1) \times \frac{N}{K} : i \times \frac{N}{K}], \quad (4)$$

Therefore,  $N$  image patches can be divided equally into  $K$  non-overlapping parts  $\mathbf{x}_{v_1}, \mathbf{x}_{v_2}, \dots$ , and  $\mathbf{x}_{v_K}$  by the indices  $\mathbf{ids}_i$ , as shown in Eq(5), where  $d(\cdot)$  denotes drawing values from input  $\mathbf{x}$  according to the specified indices  $\mathbf{ids}_i$ .

$$\mathbf{x}_{v_i} = d(\mathbf{x}, \mathbf{ids}_i), \quad (5)$$

The mask  $\mathbf{m}_i$  of any part is given with Eq(6), where  $ms(\cdot)$  obtains the mask from  $\mathbf{t}$  according to  $\mathbf{ids}_i$ .

$$\mathbf{m}_i = ms(\mathbf{t}, \mathbf{ids}_i), \quad (6)$$

---

**Algorithm 1** Pseudocode of the division of whole data in a PyTorch-like style.

---

```
# x: the input image
# K: the number of non-overlapping parts

# map an image into multiple image patches
x = patchify(x)
N, D = x.shape # length, dim

tensor = rand(N) # tensor in [0, 1]

# sort the tensor in ascending order
ids = argsort(tensor)

# acquire the position of each element
ids_tensor = argsort(ids)

# divide the whole data into K parts
for i in range(1, K+1):

    # obtain the i-th visible patches
    ids_i = ids[(i-1)*(N/K) : i*(N/K)]
    x_v_i = gather(x, dim=0, index=ids_i)

    # obtain the i-th mask
    m_i = ones(N)
    m_i[(i-1)*(N/K) : i*(N/K)] = 0
    m_i = gather(m_i, dim=0, index=ids_tensor)

    # obtain the i-th masked patches
    x_m_i = x[m_i].reshape(-1, D)
```

---

rand: returns a tensor filled with random numbers from a uniform distribution on the interval  $[0,1]$ ; gather: gathers values along an axis specified by dim; argsort: returns the indices that sort a tensor along a given dimension in ascending order by value.

Any part  $\mathbf{x}_{v_i}$  has  $N/K$  visible patches, and its corresponding complementary view  $\mathbf{x}_{m_i}$  has  $N - N/K$  masked patches, which is defined as Eq(7). Hence, the mask ratio of any part is  $(N - N/K)/K = (K - 1)/K$ . More details are described in Algorithm 1.

$$\mathbf{x}_{m_i} = \mathbf{x} \odot \mathbf{m}_i, \quad (7)$$

From the above description, image patches are progressively divided into  $K$  non-overlapping parts according to the principle of sampling without replacement [36]. When  $K$  is set to be 4, the mask ratio of each part is 75% (the same as the mask ratio of MAE). The design ensures the whole image can be applied to train the model while each patch of the image in an iteration can be sampled once, thereby enhancing the data utilization. According to our design in Figure 2, each part containing visible patches is fed as the input into the encoder-decoder architecture and performs the MIM task, and the loss function is defined as Eq(8).

$$\mathcal{L}_{whole}(\mathbf{x}) = \mathbb{E}_{i \in [1, K]} \mathcal{L}(\mathbf{x}_{v_i}, \mathbf{x}_{m_i}), \quad (8)$$

#### 3.2.2 Self-consistency module

The utilization of whole image in Section 3.2.1 enhances the global understanding of the model in an iteration, but it still can not guarantee the reliability of the output results



for each part. According to the pioneering work [27], human intelligence is a self-consistency system, which helps to efficiently learn and correct mistakes. Therefore, it is reasonable to believe that artificial models can also improve training efficiency and consistency when introducing the self-consistency mechanism. In detail, the predictions of the pre-trained model are encouraged to be consistent under different input visible patches from the same image.

In terms of Section 3.2.1, each part has  $N/K$  of the whole image and generates  $N - N/K$  predictions. The predictions of each part are  $\mathbf{x}_{p_1}, \mathbf{x}_{p_2}, \dots$ , and  $\mathbf{x}_{p_K}$ . Obviously, there is a certain ratio of overlap between the predictions for any two sets of parts, and the ratio is  $(K - 2)/(K - 1)$ . The overlapping position  $\mathbf{s}_{ij}$  of any two sets of predictions  $\mathbf{x}_{p_i}, \mathbf{x}_{p_j}$  can be obtained by the mask  $\mathbf{m}_i$  and  $\mathbf{m}_j$ , where  $i, j \in \{1, 2, \dots, K\}$  and  $i \neq j$ . The definition of  $\mathbf{s}_{ij}$  is denoted as Eq(9).

$$\mathbf{s}_{ij} = \mathbf{m}_i \cap \mathbf{m}_j, \quad (9)$$

Consequently, the self-consistency module is proposed to guide the predictions of each overlapping position to keep consistent. As shown in Figure 2, the self-consistency module pulls together the overlapping predictions between any two sets  $x_{p_i}$  and  $x_{p_j}$ , which minimizes the mean absolute error between the overlapping reconstructed results to increase consistency. The *self-consistency loss* is defined as Eq(10), where  $\text{sg}[\cdot]$  stands for stop gradient. For each prediction of any part, it will calculate with that of other parts by  $K - 2$  times.

$$\mathcal{L}_{sc}(\mathbf{x}_{v_i}, \mathbf{x}_{v_j}) = (\|\text{sg}[\mathbf{x}_{p_i}] - \mathbf{x}_{p_j}\| + \|\mathbf{x}_{p_i} - \text{sg}[\mathbf{x}_{p_j}]\|) \odot \mathbf{s}_{ij}, \quad (10)$$

Finally, the self-consistency loss of the image is calculated according to the Eq(12).

$$\mathcal{L}_{consistency}(\mathbf{x}) = \mathbb{E}_{i \in [1, K], j \in [i+1, K]} \mathcal{L}_{sc}(\mathbf{x}_{v_i}, \mathbf{x}_{v_j}), \quad (11)$$

The behavior induced by the self-consistency loss can be observed in Figure 3: the reconstructed images from different combinations end up matching closely each other.

### 3.2.3 Objective function

Our EMAE consists of the design of whole data utilization and the self-consistency module. Thus, the final loss for our EMAE can be formulated as Eq(12), each loss coefficient is set to be 1 for equally weighted.

$$\mathcal{L}_{total}(\mathbf{x}) = \mathcal{L}_{whole}(\mathbf{x}) + \mathcal{L}_{consistency}(\mathbf{x}), \quad (12)$$

### 3.3. Discussion

In this section, we present some intuitive analysis about why EMAE can improve the pre-training efficiency and increase consistency, which will be further demonstrated

Method	Arch	pre-training # epochs	ImageNet	
			LP	FT
<i>Supervised learning on ImageNet:</i>				
scratch [7]	ViT-S	300	-	79.9%
scratch [19]	ViT-B	300	-	82.3%
scratch [19]	ViT-L	300	-	82.6%
<i>Contrastive learning:</i>				
MoCo v3 [9]	ViT-B	300	76.2%	83.2%
DINO [3]	ViT-B	400	<b>78.2%</b>	<b>83.4%</b>
<i>Masked image modeling + contrastive learning:</i>				
MST [30]	ViT-S	100	75.0%	-
AttMask [25]	ViT-S	100	76.1%	81.3%
iBOT [53]	ViT-S	100	74.4%	81.1%
iBOT [53]	ViT-S	3,200	77.9%	82.3%
iBOT [53]	ViT-B	1,600	79.5%	84.0%
iBOT [53]	ViT-L	1,200	<b>81.0%</b>	<b>84.8%</b>
<i>Masked image modeling:</i>				
CAE [7]	ViT-S	300	50.8%	81.8%
CAE [7]	ViT-B	800	68.3%	83.6%
BEiT [1]	ViT-B	800	56.7%	83.2%
BEiT [1]	ViT-L	800	73.5%	85.2%
SimMIM [48]	ViT-B	800	56.7%	83.8%
MAE [19]	ViT-B	300	61.5%	82.9%
MAE [19]	ViT-B	800	64.4%	83.4%
MAE [19]	ViT-B	1600	67.8%	83.6%
MAE [19]	ViT-B	2400	68.2%	83.8%
MAE [19]	ViT-L	1600	75.6%	85.9%
MAE [19]	ViT-H	1600	76.6%	86.9%
EMAE	ViT-B	300	68.2%	83.8%
EMAE	ViT-B	800	70.4%	84.0%
<b>EMAE</b>	ViT-L	800	<b>76.7%</b>	<b>86.3%</b>

Table 1. **Comparison of SOTA self-supervised learning methods.** EMAE is pre-trained on ImageNet `train` set and achieves state-of-the-art performance than previous masked image modeling methods. For evaluation, we test the performance of the pre-trained models under two supervised training settings: 1) linear probing (LP), and 2) end-to-end fine-tuning (FT). We report top-1 accuracy on the ImageNet `val` set.

with empirical results in Section 4. The primary component that makes EMAE converge faster is the utilization of multiple non-overlapping parts, which efficiently exploits the whole image in the training stage. Thus, EMAE can get sufficient supervision signals in each epoch compared to MAE and achieves promising performance with fewer epochs. Notably, according to the principle of sampling without replacement, the whole image is divided equally into  $K$  non-overlapping parts. The design can ensure each patch in an image can be used to train the model, thus enhancing the utilization of whole data, unlike MAE. Finally, we propose the self-consistency loss to decrease the uncertainty and inconsistency of MIM. Based on the design of the whole data, the self-consistency mechanism further im-

proves feature representations, thereby benefiting the performance. Owing to these merits, EMAE can achieve high pre-training efficiency and consistent representations, thus obtaining promising performance. Experimental results in Section 4.5 below will validate these analyses.

## 4. Experiments

### 4.1. Datasets and pre-training settings

Following the setting of MAE [19], EMAE is mainly evaluated on linear probing, finetuning classification, object detection, instance segmentation, and semantic segmentation tasks. The details of our utilized datasets and experimental settings are introduced in the next.

**Datasets.** In this paper, EMAE is evaluated on the linear probing and finetuning classification task of ImageNet-1K [11], which is a popular large-scale image classification dataset with 1.28 million images and 1000 categories. Additionally, detection and segmentation are dense vision tasks, which contain massive instances inside each image. Therefore, the evaluation of dense vision tasks can better reflect the semantics capacity of pre-trained models. We conduct sufficient experiments on COCO [34] and ADE20k [52] dataset to verify the generalization and transfer ability of EMAE. COCO is a relatively challenging object detection and instance segmentation dataset, which `train2017` contains about 118k images and evaluate on the `val2017` contains 5k images. Moreover, ADE20K is also a challenging semantic segmentation dataset, and it contains 25k images of 150 categories.

**Pre-training settings.** The training settings are the same as MAE [19], we adopt the same encoder-decoder structure to perform the MIM task. Our method is general for ViT backbones, while most experiments are conducted with ViT-base, due to the limitation of computation resources. Specifically, we partition the image of  $224 \times 224$  into  $14 \times 14$  patches with the patch size being  $16 \times 16$ . The  $K$  is set to be 4 by default. The batch size is set to be 4096. Meanwhile, the weight decay,  $\beta_1$  and  $\beta_2$  for AdamW [38] is set to be 0.05, 0.9 and 0.95 respectively. We use a cosine learning rate strategy [37] with warmup [17]. The warmup number is set to be 40 epochs and the base learning rate is set to be  $base\_lr = 1.5e^{-4}$ . After the self-supervised pre-training on the ImageNet-1K is over, we evaluate the learned representation quality with only the encoder preserved. Please refer to Appendix for more details.

### 4.2. Image classification on ImageNet-1K

**Experimental setting.** For a fair comparison, we fully follow the hyperparameters of MAE [19] in our image classification experiments. We evaluate the performance of the pre-trained encoder under two supervised training settings: 1) linear probing (LP), and 2) end-to-end fine-tuning (FT).

For the linear probing, all parameters of the pre-trained encoder are frozen while only the last classification layer is trained. The LARS [49] optimizer is exploited with batch size 16,384. The ViT-base is trained with 90 epochs while the ViT-large is trained with 50 epochs. The cosine learning strategy is used with 0.1 base learning rate. Also, for the end-to-end fine-tuning, the pre-trained encoder is fine-tuned with the classification head together. For different ViT backbones, ViT-base is trained for 100 epochs while ViT-large is trained for 50 epochs, of which the base learning rate and batch size are set to  $1e^{-3}$  and 1,024, respectively. Besides, AdamW optimizer with a cosine learning rate scheduler is adopted. The weight decay is set to 0.05.

**Classification results.** As shown in Tab. 1, we surprisingly find that our method using ViT-base can surpass the MAE by around 6.0%  $\sim$  6.7% with the same pre-training epochs (300 and 800 epochs) in linear probing. The 300-epoch classification results are on par with that of the 2400-epoch MAE. The phenomenon indicates that our method can significantly improve the training efficiency of MIM. Extra training (800 epochs) further improves the linear result to 70.4% and finetuning result to 84.0%, and achieves SOTA performance. Moreover, it is noted that our 800-epoch classification results using ViT-large are comparable with that of 1600-epoch MAE using ViT-huge. As a MIM-based method, EMAE surpasses previous SOTA MIM-based methods. The linear results of EMAE are slightly inferior to contrastive-based methods due to the contrastive-based method has the assumption of image semantic consistency [31, 35], and the assumption is consistent with the prior of the linear probing task.

### 4.3. Object detection and instance segmentation

To further validate the learned visual representation of our EMAE, we perform fine-tuning on the COCO [34] object detection and instance segmentation. We choose the Mask R-CNN [21] framework. Concretely, we adopt FPNs [32] to scale the feature map into different sizes as introduced in [29]. By fully following the strategy of previous [19, 29], we conduct these experiments on COCO. The results are reported in Table 2 in terms of box AP ( $AP^b$ ) for detection and mask AP ( $AP^m$ ) for segmentation. We show the performance of the learned representation by different self-supervised methods and supervised training. We observe that our method achieves the best results with 51.4%  $AP^b$  and 45.7%  $AP^m$ , and surpasses MAE by 1.0 and 0.8 points, individually.

Besides, we also conduct experiments on the SOTA ViT-based detection framework ViTDet [28] to verify the transfer ability of MAE. For a fair comparison, all of these experiments strictly adopt the training settings of ViTDet. In Table 3, it can be observed that our EMAE outperforms MAE 1.3 and 1.2 points on  $AP^b$  and  $AP^m$ . Also, the results of

Method	Pre-train epochs	Pre-train data	Object detection			Instance segmentation		
			AP <sup>b</sup>	AP <sub>50</sub> <sup>b</sup>	AP <sub>75</sub> <sup>b</sup>	AP <sup>m</sup>	AP <sub>50</sub> <sup>m</sup>	AP <sub>75</sub> <sup>m</sup>
Supervised [7]	300	ImageNet-1K	46.9	68.9	51.0	41.5	65.5	44.4
MoCo v3 [9]	600	ImageNet-1K	47.9	-	-	42.7	-	-
BEiT [1]	800	ImageNet-1K + DALLE	49.8	-	-	44.4	-	-
CAE [7]	1600	ImageNet-1K	50.0	70.9	54.8	44.0	67.9	47.6
MAE [19]	1600	ImageNet-1K	50.4	70.8	55.7	44.9	68.3	48.9
<b>EMAE</b>	800	ImageNet-1K	<b>51.4</b>	<b>72.2</b>	<b>56.5</b>	<b>45.7</b>	<b>69.4</b>	<b>49.8</b>

Table 2. **Results of object detection and instance segmentation on COCO using Mask R-CNN [19, 29].** The architecture of various methods adopts ViT-B. We adopt Mask R-CNN [21] with FPN [32], and report the bounding box AP and mask AP on COCO val2017. EMAE outperforms the previous SOTA self-supervised learning method.

Method	Pre-train data	AP <sup>b</sup>	AP <sup>m</sup>
Rand Init [28]	-	48.1	42.6
Supervised [28]	ImageNet-1K	47.6	42.4
Supervised [28]	ImageNet-21K	47.8	42.6
MAE [20]	ImageNet-1K	51.2	45.5
MAE, <i>our impl.</i>	ImageNet-1K	51.6	45.9
<b>EMAE</b>	ImageNet-1K	<b>52.5</b>	<b>46.7</b>
MAE + cascade	ImageNet-1K	54.0	46.7
<b>EMAE + cascade</b>	ImageNet-1K	<b>54.8</b>	<b>47.6</b>

Table 3. **Results of object detection and instance segmentation fine-tuned on COCO using ViTDet [28].** For a fair comparison, the architecture of various methods adopts ViT-B. ViTDet [28] is adopted as the detection framework, and our EMAE achieves impressive performance and outperforms the previous SOTA self-supervised learning method MAE.

Method	Pre-train data	Pre-train epochs	ADE mIoU
Supervised [19]	ImageNet-1K	300	47.4
SplitMask [15]	ADE20K	21000	45.7
MoCo v3 [9]	ImageNet-1K	600	47.3
BEiT [19]	ImageNet-1K+DALLE	800	47.1
PeCo [13]	ImageNet-1K	300	46.7
CIM [16]	ImageNet-1K	100	43.5
MAE [19]	ImageNet-1K	1600	48.1
CAE [7]	ImageNet-1K	800	48.8
<b>EMAE</b>	ImageNet-1K	800	<b>49.3</b>

Table 4. **Results of semantic segmentation on ADE20K using UperNet [47].** For a fair comparison, the architecture of various methods adopts ViT-B. We report results measured by mean Intersection of Union (mIoU), and EMAE surpasses the previous self-supervised method and achieves the SOTA performance.

ViTDet with Cascade Mask RCNN reach 54.8% AP<sup>b</sup> and 47.6% AP<sup>m</sup>, and surpass MAE by 0.8 and 0.9 points, respectively. These experiments show that our EMAE can be applicable to any other detection framework to boost per-

Method	Pre-epochs			
	100	200	300	800
baseline	54.8%	58.8%	61.5%	64.4%
+ whole data utilization	60.0%	63.4%	65.3%	68.4%
<b>++ self-consistency</b>	<b>60.9%</b>	<b>65.0%</b>	<b>68.4%</b>	<b>70.4%</b>

Table 5. **Ablations for EMAE: Effect of whole data utilization and the self-consistency module.** We report the results of linear evaluation on ImageNet.

formance without additional training costs and efforts.

#### 4.4. Semantic segmentation

We also evaluate our EMAE on another dense prediction task, semantic segmentation on the ADE20K [52] dataset. The mean Intersection of Union (mIoU) averaged over all semantic categories is reported as the evaluation metric. In particular, by fully following the training settings of MAE, we adopt UperNet framework [47] in our experiments and report the results in Table 4. We compare our method with supervised pre-training on ImageNet-1K as well as SOTA self-supervised methods. It can be observed that the proposed EMAE achieves the highest 49.3% mIoU and gets superior performance than all the other baselines, further validating the effectiveness of our framework.

#### 4.5. Ablation studies

To better investigate the effectiveness of different components in our proposed EMAE, we conduct ablation studies on ImageNet-1K dataset. Linear probing is still an excellent evaluation method to quickly validate the learned representations, and MAE also selects the mask ratio according to the performance of linear probing. Hence, we adopt the results of linear probing as our benchmark for measuring effectiveness in ablation studies. For a fair comparison, the architecture of various methods adopts ViT-base.

**Effect of whole data utilization.** In Section 3.2.1, we have discussed the superiority of whole data utilization. As shown in Table 5, the second line shows the results of MAE pre-training on ImageNet dataset for different pre-training

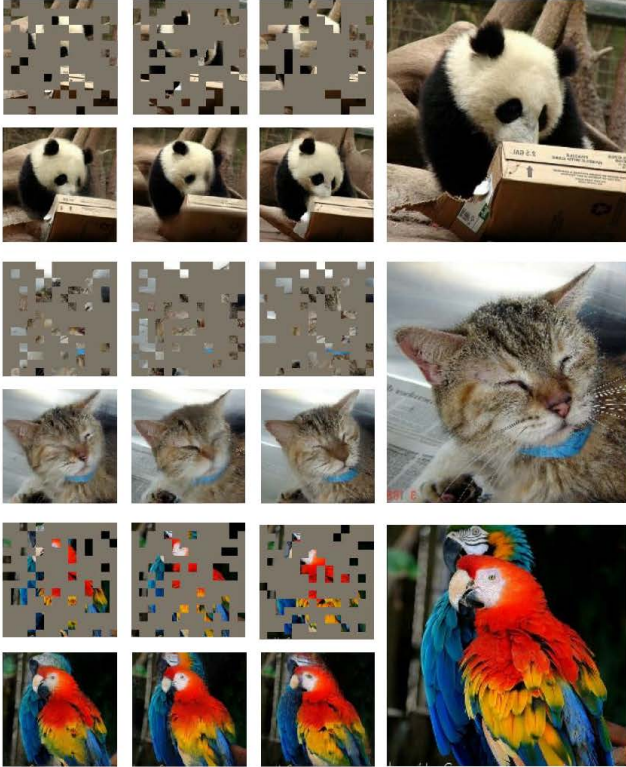


Figure 3. **Different reconstruction results of our EMAE correspond to different mask seeds.** Different combinations of visible patches are sampled from the same image by the random seeds, then these combinations are fed into our EMAE and EMAE generates the reconstructed images. Here, we reconstruct three images as examples. These reconstruction results contain similar semantics and become matched closely with each other, demonstrating the effectiveness of our self-consistency module.

epochs (e.g., 100, 200, 300, and 800 pre-training epochs) as our baseline. The third line indicates that the whole data is divided into 4 non-overlap parts under different pre-training epochs. Compared with the baseline, the results of the third line surpass the MAE by around 4.0% ~ 5.2% with the same pre-training epochs, demonstrating that sufficient training data can effectively improve performance. Moreover, these results illustrate the importance of exploiting the whole data, which can efficiently increase data utilization and improve pre-training efficiency.

**Effect of the self-consistency module.** To further improve consistency, we propose the self-consistency module to encourage the model to generate reliable representations in the pre-training process. On the basis of the whole data utilization design, the self-consistency loss is introduced to the training stage, and the results are listed in the fourth line of Table 5. Compared with the whole data utilization design, the results of the fourth line further enhance the performance of the pre-trained model, e.g., the results

Method \ Pre-epochs	100	300	800
(a) MAE mask ratio = $\frac{3}{4}$	54.8%	61.5%	64.4%
(b) EMAE K = 4	60.9%	68.4%	70.4%
(c) MAE mask ratio = $\frac{6}{7}$	53.3%	61.0%	63.9%
(d) EMAE K = 7	60.5%	66.5%	68.1%
(e) MAE mask ratio = $\frac{13}{14}$	46.4%	54.7%	60.7%
(f) EMAE K = 14	52.5%	61.0%	66.7%

Table 6. **Ablations for EMAE: Effect of the K division.** We report the results of linear evaluation on ImageNet.

of the fourth line surpass that of the third line by around 0.9% ~ 2.9% with the same pre-training epochs. Hence, EMAE outperforms the MAE by around 6.0% ~ 6.7% with the same pre-training epochs. Notably, after the self-consistency module is introduced to the model, it can be observed that the reconstructed images generated by our EMAE end up matching closely each other in Figure 3. From the above description, it illustrates the effectiveness and superiority of the self-consistency mechanism, which further improves the performance and efficiency of MIM.

**Effect of the K division.** According to Section 3.2.1, the K directly determines the mask ratio of each part, and the mask ratio is  $\frac{K-1}{K}$ . In Table 6, it can be observed that our approach constantly surpasses the MAE with different mask ratios (e.g.,  $\frac{3}{4}$ ,  $\frac{6}{7}$ , and  $\frac{13}{14}$  mask ratios) in the same pre-training settings. Meanwhile, the performance of our approach acquires the best when the K is set to be 4 (the mask ratio is 75%), and the phenomenon also fits the observation of MAE about the mask ratio.

## 5. Conclusion

In this paper, we investigate the two serious problems caused by the high mask ratio of masked image modeling, namely inefficient pre-training and the high inconsistency of the pre-trained model. To overcome the above problems, we propose an approach, called efficient masked autoencoders with self-consistency (EMAe). The proposed EMAe exploits the whole data to perform the self-supervised task, which improves the data utilization, and thus enhances the pre-training efficiency. At the same time, the self-consistency module is proposed to decrease the uncertainty and inconsistency of masked image modeling, which further improves the performance. The proposed EMAe shows good versatility and scalability in multiple downstream visual tasks, such as linear evaluation, finetuning classification, object detection, instance segmentation, and semantic segmentation. We expect that our study can attract the community’s attention to more efficient and reliable masked image modeling.

**Limitations and social impacts.** In this work, we validate the performance of EMAe by constructing experi-



ments on ImageNet dataset. However, the promise of self-supervised learning is to establish a general feature extractor with larger datasets. We have not extended this method to larger datasets [43, 44, 51] and larger architectures (e.g., ViT-H) due to the resource and time consumption. Meanwhile, EMAE predicts content based on learned statistics of the training dataset and as such will reflect biases in those data, including ones with negative social impacts. These limitations warrant further research and consideration when building upon this work to achieve a better self-supervised learning method.

## References

- [1] Hangbo Bao, Li Dong, and Furu Wei. Beit: Bert pre-training of image transformers. *arXiv preprint arXiv:2106.08254*, 2021. 1, 2, 3, 5, 7
- [2] Mathilde Caron, Ishan Misra, Julien Mairal, Priya Goyal, Piotr Bojanowski, and Armand Joulin. Unsupervised learning of visual features by contrasting cluster assignments. In *Advances in Neural Information Processing Systems*, volume 33, pages 9912–9924, 2020. 1, 2
- [3] Mathilde Caron, Hugo Touvron, Ishan Misra, Hervé Jégou, Julien Mairal, Piotr Bojanowski, and Armand Joulin. Emerging properties in self-supervised vision transformers. *arXiv: Computer Vision and Pattern Recognition*, 2021. 2, 5
- [4] Mark Chen, Alec Radford, Rewon Child, Jeffrey K Wu, Heewoo Jun, David Luan, and Ilya Sutskever. Generative pre-training from pixels. In *ICML*, volume 1, pages 1691–1703, 2020. 1, 2, 3
- [5] Ting Chen, Simon Kornblith, Mohammad Norouzi, and Geoffrey Hinton. A simple framework for contrastive learning of visual representations. *arXiv preprint arXiv:2002.05709*, 2020. 1, 2
- [6] Ting Chen, Simon Kornblith, Kevin Swersky, Mohammad Norouzi, and Geoffrey E. Hinton. Big self-supervised models are strong semi-supervised learners. In *Advances in Neural Information Processing Systems*, volume 33, pages 22243–22255, 2020. 1, 2
- [7] Xiaokang Chen, Mingyu Ding, Xiaodi Wang, Ying Xin, Shentong Mo, Yunhao Wang, Shumin Han, Ping Luo, Gang Zeng, and Jingdong Wang. Context autoencoder for self-supervised representation learning. *arXiv preprint arXiv:2202.03026*, 2022. 5, 7
- [8] Xinlei Chen, Haoqi Fan, Ross Girshick, and Kaiming He. Improved baselines with momentum contrastive learning. *arXiv preprint arXiv:2003.04297*, 2020. 1, 2
- [9] Xinlei Chen, Saining Xie, and Kaiming He. An empirical study of training self-supervised vision transformers. *arXiv preprint arXiv:2104.02057*, 2021. 2, 5, 7
- [10] Zhiyang Chen, Yousong Zhu, Zhaowen Li, Fan Yang, Wei Li, Haixin Wang, Chaoyang Zhao, Liwei Wu, Rui Zhao, Jinqiao Wang, et al. Obj2seq: Formatting objects as sequences with class prompt for visual tasks. *arXiv preprint arXiv:2209.13948*, 2022. 2
- [11] Jia Deng, Wei Dong, Richard Socher, Li-Jia Li, Kai Li, and Li Fei-Fei. Imagenet: A large-scale hierarchical image database. In *CVPR*, 2009. 2, 6
- [12] Jacob Devlin, Ming-Wei Chang, Kenton Lee, and Kristina N. Toutanova. Bert: Pre-training of deep bidirectional transformers for language understanding. In *Proceedings of the 2019 Conference of the North American Chapter of the Association for Computational Linguistics: Human Language Technologies, Volume 1 (Long and Short Papers)*, pages 4171–4186, 2018. 1, 2
- [13] Xiaoyi Dong, Jianmin Bao, Ting Zhang, Dongdong Chen, Weiming Zhang, Lu Yuan, Dong Chen, Fang Wen, and Nenghai Yu Peco. Perceptual codebook for bert pre-training of vision transformers. *arXiv preprint arXiv:2111.12710*, 1(3):7, 2021. 7
- [14] Alexey Dosovitskiy, Lucas Beyer, Alexander Kolesnikov, Dirk Weissenborn, Xiaohua Zhai, Thomas Unterthiner, Mostafa Dehghani, Matthias Minderer, Georg Heigold, Sylvain Gelly, Jakob Uszkoreit, and Neil Houlsby. An image is worth 16x16 words: Transformers for image recognition at scale. In *ICLR*, 2021. 1, 2, 3
- [15] Alaaeldin El-Nouby, Gautier Izacard, Hugo Touvron, Ivan Laptev, Hervé Jegou, and Edouard Grave. Are large-scale datasets necessary for self-supervised pre-training? *arXiv preprint arXiv:2112.10740*, 2021. 7
- [16] Yuxin Fang, Li Dong, Hangbo Bao, Xinggang Wang, and Furu Wei. Corrupted image modeling for self-supervised visual pre-training. *arXiv preprint arXiv:2202.03382*, 2022. 7
- [17] Priya Goyal, Piotr Dollár, Ross Girshick, Pieter Noordhuis, Lukasz Wesolowski, Aapo Kyrola, Andrew Tulloch, Yangqing Jia, and Kaiming He. Accurate, large mini-batch sgd: Training imagenet in 1 hour. *arXiv preprint arXiv:1706.02677*, 2017. 6
- [18] Jean-Bastien Grill, Florian Strub, Florent Altché, Corentin Tallec, Pierre H. Richemond, Elena Buchatskaya, Carl Doersch, Bernardo Avila Pires, Zhaohan Daniel Guo, Mohammad Gheshlaghi Azar, Bilal Piot, Koray Kavukcuoglu, Rémi Munos, and Michal Valko. Bootstrap your own latent: A new approach to self-supervised learning. In *NeurIPS*, volume 33, pages 21271–21284, 2020. 1, 2
- [19] Kaiming He, Xinlei Chen, Saining Xie, Yanghao Li, Piotr Dollár, and Ross Girshick. Masked autoencoders are scalable vision learners. *arXiv preprint arXiv:2111.06377*, 2021. 1, 2, 3, 5, 6, 7
- [20] Kaiming He, Haoqi Fan, Yuxin Wu, Saining Xie, and Ross Girshick. Momentum contrast for unsupervised visual representation learning. *arXiv preprint arXiv:1911.05722*, 2019. 1, 2, 7
- [21] Kaiming He, Georgia Gkioxari, Piotr Dollár, and Ross Girshick. Mask r-cnn. In *ICCV*, 2017. 2, 6, 7
- [22] Kaiming He, Xiangyu Zhang, Shaoqing Ren, and Jian Sun. Deep residual learning for image recognition. In *CVPR*, 2016. 2
- [23] R Devon Hjelm, Alex Fedorov, Samuel Lavoie-Marchildon, Karan Grewal, Phil Bachman, Adam Trischler, and Yoshua Bengio. Learning deep representations by mutual information estimation and maximization. *ICLR*, 2019. 1, 2

- [24] Tianyu Hua, Yonglong Tian, Sucheng Ren, Hang Zhao, and Leonid Sigal. Self-supervision through random segments with autoregressive coding (randsac). *arXiv preprint arXiv:2203.12054*, 2022. 3
- [25] Ioannis Kakogeorgiou, Spyros Gidaris, Bill Psomas, Yannis Avrithis, Andrei Bursuc, Konstantinos Karantzas, and Nikos Komodakis. What to hide from your students: Attention-guided masked image modeling. *arXiv preprint arXiv:2203.12719*, 2022. 5
- [26] Nikos Komodakis and Spyros Gidaris. Unsupervised representation learning by predicting image rotations. In *International Conference on Learning Representations (ICLR)*, 2018. 2
- [27] Prescott Lecky. Self-consistency; a theory of personality. 1945. 5
- [28] Yanghao Li, Hanzi Mao, Ross Girshick, and Kaiming He. Exploring plain vision transformer backbones for object detection. *arXiv preprint arXiv:2203.16527*, 2022. 2, 6, 7
- [29] Yanghao Li, Saining Xie, Xinlei Chen, Piotr Dollar, Kaiming He, and Ross Girshick. Benchmarking detection transfer learning with vision transformers. *arXiv preprint arXiv:2111.11429*, 2021. 6, 7
- [30] Zhaowen Li, Zhiyang Chen, Fan Yang, Wei Li, Yousong Zhu, Chaoyang Zhao, Rui Deng, Liwei Wu, Rui Zhao, Ming Tang, and Jinqiao Wang. Mst: Masked self-supervised transformer for visual representation. In *NeurIPS*, 2021. 1, 2, 5
- [31] Zhaowen Li, Yousong Zhu, Fan Yang, Wei Li, Chaoyang Zhao, Yingying Chen, Zhiyang Chen, Jiahao Xie, Liwei Wu, Rui Zhao, et al. Univip: A unified framework for self-supervised visual pre-training. *arXiv preprint arXiv:2203.06965*, 2022. 2, 6
- [32] Tsung-Yi Lin, Piotr Dollar, Ross Girshick, Kaiming He, Bharath Hariharan, and Serge Belongie. Feature pyramid networks for object detection. In *2017 IEEE Conference on Computer Vision and Pattern Recognition (CVPR)*, pages 936–944, 2017. 6, 7
- [33] Tsung-Yi Lin, Priya Goyal, Ross Girshick, Kaiming He, and Piotr Dollar. Focal loss for dense object detection. *IEEE Transactions on Pattern Analysis and Machine Intelligence*, 42(2):318–327, 2020. 2
- [34] Tsung-Yi Lin, Michael Maire, Serge Belongie, James Hays, Pietro Perona, Deva Ramanan, Piotr Dollár, and C Lawrence Zitnick. Microsoft coco: Common objects in context. In *ECCV*, 2014. 2, 6
- [35] Songtao Liu, Zeming Li, and Jian Sun. Self-emd: Self-supervised object detection without imagenet. *arXiv preprint arXiv:2011.13677*, 2020. 2, 6
- [36] Michel Loeve. *Probability theory*. Courier Dover Publications, 2017. 4
- [37] Ilya Loshchilov and Frank Hutter. Sgdr: Stochastic gradient descent with warm restarts. *arXiv preprint arXiv:1608.03983*, 2016. 6
- [38] Ilya Loshchilov and Frank Hutter. Decoupled weight decay regularization. *arXiv preprint arXiv:1711.05101*, 2017. 6
- [39] Mehdi Noroozi and Paolo Favaro. Unsupervised learning of visual representations by solving jigsaw puzzles. In *ECCV*, 2016. 2
- [40] Aaron van den Oord, Yazhe Li, and Oriol Vinyals. Representation learning with contrastive predictive coding. *arXiv preprint arXiv:1807.03748*, 2018. 1, 2
- [41] Deepak Pathak, Philipp Krahenbuhl, Jeff Donahue, Trevor Darrell, and Alexei A Efros. Context encoders: Feature learning by inpainting. In *CVPR*, 2016. 2
- [42] Shaoqing Ren, Kaiming He, Ross Girshick, and Jian Sun. Faster r-cnn: Towards real-time object detection with region proposal networks. In *NeurIPS*, 2015. 2
- [43] Chen Sun, Abhinav Shrivastava, Saurabh Singh, and Abhinav Gupta. Revisiting unreasonable effectiveness of data in deep learning era. In *Proceedings of the IEEE international conference on computer vision*, pages 843–852, 2017. 9
- [44] Bart Thomee, David A Shamma, Gerald Friedland, Benjamin Elizalde, Karl Ni, Douglas Poland, Damian Borth, and Li-Jia Li. Yfcc100m: The new data in multimedia research. *Communications of the ACM*, 59(2):64–73, 2016. 9
- [45] Aaron Van Den Oord, Oriol Vinyals, et al. Neural discrete representation learning. *Advances in neural information processing systems*, 30, 2017. 3
- [46] Zhirong Wu, Yuanjun Xiong, Stella X Yu, and Dahua Lin. Unsupervised feature learning via non-parametric instance discrimination. In *CVPR*, 2018. 1, 2
- [47] Tete Xiao, Yingcheng Liu, Bolei Zhou, Yuning Jiang, and Jian Sun. Unified perceptual parsing for scene understanding. In *Proceedings of the European Conference on Computer Vision (ECCV)*, pages 418–434, 2018. 2, 7
- [48] Zhenda Xie, Zheng Zhang, Yue Cao, Yutong Lin, Jianmin Bao, Zhuliang Yao, Qi Dai, and Han Hu. Simmim: A simple framework for masked image modeling. *arXiv preprint arXiv:2111.09886*, 2021. 1, 2, 5
- [49] Yang You, Igor Gitman, and Boris Ginsburg. Large batch training of convolutional networks. *arXiv preprint arXiv:1708.03888*, 2017. 6
- [50] Richard Zhang, Phillip Isola, and Alexei A Efros. Colorful image colorization. In *European conference on computer vision*, pages 649–666. Springer, 2016. 2
- [51] Bolei Zhou, Agata Lapedriza, Aditya Khosla, Aude Oliva, and Antonio Torralba. Places: A 10 million image database for scene recognition. *IEEE transactions on pattern analysis and machine intelligence*, 40(6):1452–1464, 2017. 9
- [52] Bolei Zhou, Hang Zhao, Xavier Puig, Tete Xiao, Sanja Fidler, Adela Barriuso, and Antonio Torralba. Semantic understanding of scenes through the ade20k dataset. *International Journal of Computer Vision*, 127(3):302–321, 2019. 2, 6, 7
- [53] Jinghao Zhou, Chen Wei, Huiyu Wang, Wei Shen, Cihang Xie, Alan Yuille, and Tao Kong. ibot: Image bert pre-training with online tokenizer. *arXiv preprint arXiv:2111.07832*, 2021. 1, 2, 5